PHYSICAL REVIEW B **84**, 041409(R) (2011)

Straining topological insulators as a way to detect Majorana fermions

Andrej Mesaros,[1,2] Stefanos Papanikolaou,[2] and Jan Zaanen[1]
[1]*Instituut-Lorentz for Theoretical Physics, Universiteit Leiden, P.O. Box 9506, NL-2300 R A Leiden, The Netherlands*
[2]*LASSP, Physics Department, Clark Hall, Cornell University, Ithaca, New York 14853-2501, USA*
(Received 2 June 2011; published 28 July 2011)

We propose the experimental setup of an interferometer for the observation of neutral Majorana fermions on topological insulator-superconductor-ferromagnet junctions. We show that the extended lattice defects naturally present in materials, dislocations, induce spin currents on the edges while keeping the bulk time-reversal symmetry intact. We propose a simple two-terminal conductance measurement in an interferometer formed by two edge point contacts, which reveals the nature of Majorana states through the effect of dislocations. The zero-temperature magneto-conductance changes from *even* oscillations with period $\phi_0/2$ (ϕ_0 is the flux quantum hc/e) to *odd* oscillations with period ϕ_0, when nontrivial dislocations are present and the Majorana states are sufficiently strongly coupled. Additionally, the conductance acquires a notable asymmetry as a function of the incident electron energy, due to the topological influence of the dislocations, while resonances appear at the coupling energy of Majorana states.

DOI: 10.1103/PhysRevB.84.041409 PACS number(s): 05.60.Gg, 03.75.Lm, 72.10.−d, 73.21.−b

There is a strong interest to realize, observe, and manipulate Majorana fermions, because of the non-Abelian statistics they possess,[1] being the basis for topological quantum computation.[2] Majorana fermions have been argued to be present in the $\nu = 5/2$ fractional quantum Hall state,[1,3] in the p-wave superconductor Sr_2RuO_4 (Ref. 4), and in topological insulator-superconductor junctions.[5,6] Topological insulators (TIs)[7] have gapless edge (2DTI) or surface (3DTI) states that are helical and topologically protected in the absence of time-reversal symmetry (TRS) breaking fields. Breaking TRS by depositing an insulating magnetic (M) material can open an energy gap leading to a surface quantum Hall effect with $\sigma_{xy} = \pm e^2/2h$ (Ref. 8). Further, deposition of a superconductor (S) on the edge or surface leads to Majorana bound states (MBSs) at an S-TI-M interface where the gap changes sign.[5] These Majorana fermions have proven to be very elusive since they are neutral, and there are a few proposals for their observation, ranging from rather indirect tunneling experiments[9] to interference experiments.[10–12] In this Rapid Communication, we make a step further and propose an interferometer which preserves TRS and can be used not only for identifying the Majoranas, but also for the dual purpose of understanding the fundamental properties of topological lattice defects.

We propose a standard Aharonov-Bohm (AB) interferometer [Fig. 1(b)], where the presence of dislocations within the interferometer area causes a topological phase shift on the edge states due to the translational effect of the dislocation Burgers vector on the edge wave function. This AB effect[13] is analogous to the effect of pierced magnetic flux,[10] except that it *preserves* TRS. The magnetic flux induces electrical current flow, the persistent current, in the ground state. Analogously, dislocations induce the TRS invariant counterpart, *dissipationless spin currents*. Spin currents are typically hard to observe, but appear useful for MBS detection. Dislocations in 3DTI were also found to host interesting states.[14]

The STIM interface locally breaks TRS and particle-hole symmetry (PHS),[5,6] so that clear experimental signatures in the two-terminal AB interferometer are expected, for example, asymmetry of the magnetoconductance [$G(\phi) \neq G(-\phi)$, where ϕ is the threaded magnetic flux] being typically absent due to TRS. We find that magnetoconductance remains *even* in the presence of MBS, due to the topological *helicity* symmetry (exchange of the left/right-moving up/down-spin, for the left/right-moving down/up-spin edge modes). However, when dislocations are present [this is controlled by straining the bulk of the TI; Fig. 1(a)], a spin current is introduced in the interferometer which is sensitive to the helicity flip and therefore can detect the signatures of MBSs. Most strikingly, the oscillations $\delta G(\phi)$ switch from *even* with period $\phi_0/2$ (ϕ_0 is the flux quantum hc/e) to *odd* oscillations with period ϕ_0 when dislocations enter the device and the MBSs are coupled (Fig. 3), while oscillations vanish in the absence of MBS at the STIM. We predict that the conductance satisfies

$$G(\phi, E, \phi_d) = G(-\phi, -E, -\phi_d) \tag{1}$$

(where E is incident electron energy and ϕ_d the dislocation scattering topological phase), which allows the use of the topological effect of dislocations (ϕ_d) as a new control parameter (absent in all existing proposals[10–12]) to bring out the signatures of the MBSs.

In the example of 2DTI realized in Hg(Cd)Te quantum wells,[7,15] dislocations seem neatly controllable. According to detailed structure studies as in Ref. 16, at low temperatures and at the yield stress of $\simeq$10–100 MPa, there are 10^{-10} m^{-2} dislocations, giving $\lesssim$1 mobile dislocations piercing a 5-μm × 5-μm sample. After yielding, no additional stress is needed in Hg(Cd)Te to move defects, so they move freely and independently. Upon reaching a high 10% strain, with a total Burgers vector of 2×10^{-9} m, one expects that $\simeq$150 dislocations have passed (glided) through such a sample. With dislocations being the most natural and abundant topological defects in crystals, we further expect the rightful use of dislocation-induced spin currents as TRS probes in the future.

Our interferometer is made of a 2DTI shaped by two point contacts [Fig. 1(b)], and we model it using the Landauer-Büttiker scattering matrix formalism valid at low temperatures in the regime of coherent transport.[17] Edge segments

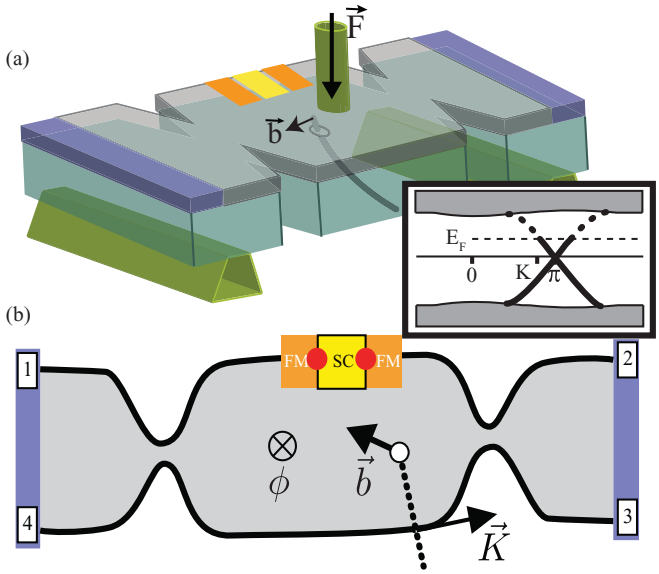

FIG. 1. (Color) Experimental setup for observing neutral Majorana fermion bound states (MBS). (a) Three-point bending (by force $\vec{F}$), moving an example dislocation line (Burgers vector $\vec{b}$) which pierces the substrate (green) and the 2D topological insulator (TI, gray) at the circle. At one TI edge there is a pair of superconductor (SC, yellow strip)-ferromagnet (FM, orange strip)-TI junctions. Contacts are marked violet. (b) Edge modes of the 2DTI (gray area) traverse the interferometer, where the MBSs (red dots) are present in the upper arm. The dislocation induces a translation on the half plane of missing atoms (dotted line), causing a topological phase shift $\exp(i\vec{K}\cdot\vec{b})$, where $\vec{K}$ is the three-dimensional embedding of the edge Fermi momentum K. (Inset) Schematic 2DTI band structure showing K near π.

comprising the interferometer support one electron and one hole *chiral* mode. The Bogoliubov–de Gennes Hamiltonian describing each edge segment is

$$\tau_3(v_F\hat{p}\,\sigma_3 + A_d + \tau_3\sigma_3 eA/\hbar c - E_F)\Psi = E\Psi, \qquad (2)$$

where $\hat{p}\equiv -i\hbar\partial/\partial x$, E_F the Fermi energy, v_F the Fermi velocity, and A the magnetic vector potential, and the x axis is along the given edge segment. The four-component spinor is $\Psi=(\Psi_{e\uparrow},\Psi_{e\downarrow},\Psi_{h\uparrow},\Psi_{h\downarrow})^T$ while the τ matrices mix the electron and hole parts of the wave function and σ the spin components.

The effect of dislocations is contained in the potential A_d of Eq. (2). It encodes for the AB effect $\exp(\frac{i}{\hbar v_F}\oint A_d\,dx)=\exp(i2\pi\phi_d)$, with pseudoflux ϕ_d stemming from the topological effect of the dislocation on the wave functions on the edge. It is well known that this effect is described by a *translation* by the Burgers vector $\vec{b}$ on traversal of electron around the dislocation core line threading the TI inside the ring-shaped area of the interferometer.[18] The translation operator $\exp(i\vec{K}\cdot\vec{b})\equiv\exp(i2\pi\phi_d)$ is determined by the three-dimensional Burgers vector $\vec{b}$ of the dislocation line that can be of any type (edge, screw, or mixed). The vector $\vec{K}$ is the three-dimensional embedding of the edge wave function wave vector K[7] [see Fig. 1(a)]. The dislocation effects discussed in this Rapid Communication depend on one-dimensional momentum K on the edge being nonzero; such 2DTI variety is not yet observed, but it could exist in Hg(Cd)Te[19] or Heusler alloys.[20] Dislocations preserve time-reversal and particle-hole (PHS) symmetries, represented by $T=i\sigma_2 C$ and $\Xi=\tau_2\sigma_2 C$, respectively, with C the complex conjugation, and they are distinct from ordinary disorder due to their intrinsic gauge symmetry. Generically, as in HgTe wells, edge segments do not exhibit PHS, so we checked that our results are robust to breaking PHS by assigning different velocities to edge states below and above $E=0$ (e.g., the edge energy spectrum observed in 3DTI[21]).

Scattering formalism. The Hamiltonian of Eq. (2) determines the energy-dependent wave vector of the left (spin-down on upper edge)-moving and right (spin-up on upper edge)-moving electrons, as well as their time-reversed hole pairs. The point contacts, the two halves of the upper ring arm, the coupled MBSs between the two upper arm halves, and the lower ring arm are all described by single scattering points with corresponding matrices ($S_{\rm scatt}$). Each matrix $S_{\rm scatt}$ connects the amplitudes ($\boldsymbol{O}_L$ and $\boldsymbol{O}_R$) of the modes *outgoing* to the left/right (L/R) side, to the amplitudes ($\boldsymbol{I}_L$ and $\boldsymbol{I}_R$) of the *incoming* modes, with respect to that particular scatterer. Using $O^T=(\boldsymbol{o}_L,\boldsymbol{o}_R)^T=(o^L_{e\downarrow},o^L_{h\uparrow},o^R_{e\uparrow},o^R_{h\downarrow})^T$ and $I^T=(\boldsymbol{I}_L,\boldsymbol{I}_R)^T=(i^L_{e\uparrow},i^L_{h\downarrow},i^R_{e\downarrow},i^R_{h\uparrow})^T$ we have $O=S_{\rm scatt}I$. The matrices have a block structure $S_{\rm scatt}=\left(\begin{smallmatrix} r & t'\\ t & r'\end{smallmatrix}\right)$, representing reflection (r, r') and transmission (t, t'), where each block has electron/hole components, for example, $t=\left(\begin{smallmatrix} t^{\rm ee} & t^{\rm he}\\ t^{\rm he} & t^{\rm hh}\end{smallmatrix}\right)$. When TRS is obeyed, backscattering is forbidden in the single-particle formalism, $r=r'=0$.[22] We compute the total scattering matrix S for the four leads [labeled from 1 to 4, Fig. 1(b)], determining the conductance of the device.

Particle conservation is enforced by $S^\dagger S=\mathbb{1}$. For scattering matrices connecting two edge segments, TRS demands $S_{\rm scatt}(\phi)=-\alpha_3 S_{\rm scatt}(-\phi)^T\alpha_3$, and PHS $S_{\rm scatt}(E)=\beta_1 S_{\rm scatt}(-E)^*\beta_1$, where α and β are Pauli matrices acting on the L/R and e/h indices of $S_{\rm scatt}$, respectively. For scattering involving all four edges (like in S) one should only replace α by $\alpha\otimes\alpha'$, where α' matrices exchange the two leads on the same side (i.e., 1 and 4, or 2 and 3). The scattering caused by the coupling to and propagation through the two MBSs in the upper arm is given by the scattering matrix S_{MBS} found in Ref. 6. It is determined by two energy scales, the coupling between the two MBSs E_M, and the coupling of edge states to the MBSs Γ. Length is measured in units of the ring circumference L, ϕ in units of the flux quantum $\phi_0=hc/e$, and energy in units of $\hbar v_F/L$. We consider the scattering mechanisms as follows. (a) Propagation in the lower arm $S_{\rm low}$ is determined by nonzero elements $t^{ee}_{\rm low}=\exp[il_d(E+2\pi\phi_d-2\pi\phi)]$, $t^{hh}_{\rm low}=\exp[il_d(E-2\pi\phi_d+2\pi\phi)]$, where l_d is the length of the lower arm. (b) In the upper arm segments $S_{\rm up}=S^T_{\rm low}$, with l_d replaced with l_{u1} and l_{u2} in the two segments, respectively. (c) Without loss of generality we take the point contact scattering matrix $S_{\rm PC}$ to be real and satisfying the TRS and PHS symmetries [edge segments are ordered as (1,4) on the left and (2,3) on right, cf. Fig. 1]:

$$S_{\rm PC}=\begin{pmatrix} 0 & a & b & b'\\ a & 0 & -b' & b\\ b & b' & 0 & -a\\ -b' & b & -a & 0\end{pmatrix}\otimes\beta_0, \qquad (3)$$

with $\beta_0 = \mathbb{1}$ and $a^2 + b^2 + b'^2 = 1$. Parameter a describes the coupling of the ring-shaped middle of the interferometer to the leads ($a = 0$ corresponds to an isolated ring with $G = 0$). The ratio $\epsilon \equiv b/b'$ measures the asymmetry of current injected into the lower and upper ring arms ($\epsilon = 0$ corresponds to all particles from lead 1 being injected into the lower arm, and all from lead 4 into the upper). Following Refs. 23, in the present single particle scattering we attain the conductance of the charge-conductor/spin-insulator (CI) state by choosing $a = 1/\sqrt{3}$, $\epsilon = 1$, being in the regime of Luttinger liquid coupling $g_c > 2$. In the realistic case of intermediate $0 < a < 1$, the dependence on a and ϵ is weak, so we present results for CI contacts. The conductance is given by $G = e^2/h \sum_{\substack{i=1,4 \\ j=2,3}} (|S_{ij}^{ee}|^2 - |S_{ij}^{he}|^2)$, where i, j label the leads, and holes contribute opposite-charge current from electrons. The zero-temperature conductance at zero voltage corresponds to taking $E = 0$, while at low temperature and voltage difference, E is given by the external voltage ($E = eV_1$). We consider $E_F = 0$ (small E_F is negligible when $K \simeq \pi$; see inset Fig. 1) and fix $l_{u1} = l_{u2} = l_d/2 = L/2$, while the results are insensitive to the asymmetry in l_{u1} and l_{u2}. The point contact parameters a, ϵ are set to be the same in the left and right contacts since results are robust to this asymmetry too.

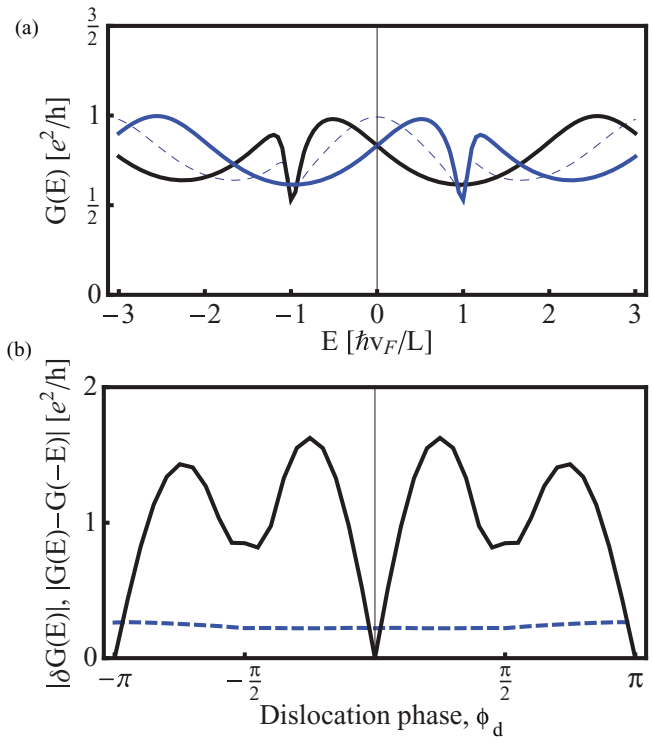

FIG. 2. (Color online) The energy (voltage)-dependent conductance, as a function of dislocation, with $E_M = 1$. (a) Typical curves: no dislocation (dashed thin line); dislocation phase $\phi_d = 0.1$ (thick black); and $\phi_d = -0.1$ [thick light gray (blue)]. Note the resonances at $\pm E_M = \pm 1$ and the dislocation-induced asymmetry. (b) The asymmetry of the $G(E)$ curves (full black line), calculated as $Max_E[G(E) - G(-E)]$ on the interval $E \in [0,3]$ [it reaches 2 for purely odd $G \sim \sin(E)$]. The dashed gray (blue) line shows the amplitude of $G(E)$ oscillations around the mean. The curves are robust to changes in E_M.

The symmetry expressed in Eq. (1) is most revealing since it controls the behavior of the conductance $G(\phi, E)$, given the changes in the net Burgers vector d. It represents the invariance of the edge states to switching the spin orientation of left- and right-moving carriers. (This orientation is set by the sign of the bulk spin-orbit coupling.) For the scattering on the edge, this switch is represented by conjugation C, that is, the combined time-reversal and spin-flip operation. In this case, it follows that $S_{\rm scatt}(E) = S_{\rm scatt}(-E)^*$ and nontrivially for the case of S_{MBS}, this property holds because $H_M^* = -H_M$. The two-level Hamiltonian H_M fundamentally obeys the relation because the Majorana fields are real ($\gamma_a^\dagger = \gamma_a$). We expect the spin-flip symmetry to be robust in absence of Zeeman-type coupling to out-of-plane magnetic fields.

We first consider the effect of dislocations on a trivial interferometer, one without a STIM interface. The presence of $\phi_d \neq 0$ introduces a deviation from evenness in $G(E)$, as the symmetry $G(E,\phi_d) = G(-E, -\phi_d)$ suggests. The magnetoconductance $G(\phi) = G(-\phi)$ stays even, protected by TRS in a two-terminal measurement. However, the nature of the $G(\phi)$ oscillations switches from dominantly universal conductance fluctuations (UCFs), that is, period ϕ_0, to a dominantly period $\phi_0/2$ nature, when dislocation is introduced.

Second, we introduce the STIM interface into the upper arm of the interferometer (cf. Fig. 1). If there are *no* MBSs forming, the STIM is a segment of gapped edge states with a TRS violation. The absence of MBS is modeled by setting $\Gamma = 0$ (decoupling from the edges). In this case, the magnetoconductance oscillations $\delta G(\phi)$ vanish. The dislocations influence the oscillations, and $G(E,\phi_d) = f(E - \phi_d)$, with $f(x) = b'^2(1 - a^4)[(1 + a^2)(1 + \epsilon^2) + 4a\epsilon \cos(x/2)]/[1 + a^8 + 2a^4 \cos(2x)]$ shows

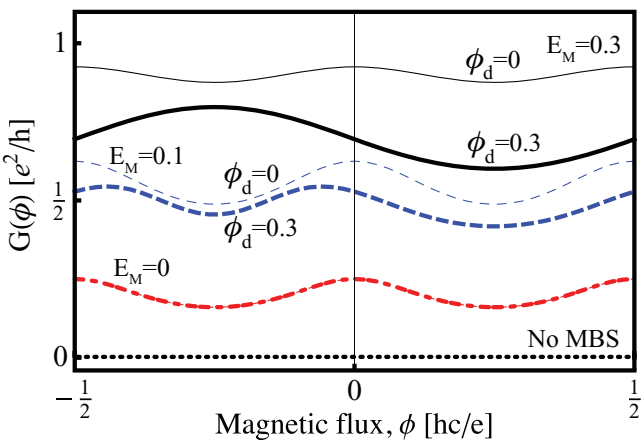

FIG. 3. (Color online) Magnetoconductance $G(\phi)$ at zero energy (voltage) as function of dislocations and Majorana couplings. In the absence of MBS, $G(\phi)$ vanishes (dotted black line). The dash-dotted (red), dashed (blue), and solid (black) curves correspond to three regimes of MBS coupling $E_M = 0, 0.1, 0.3$, respectively, with respect to MBS-edge coupling $\Gamma = 0.1$ (units $\hbar v_F/L$). The case of absence ($\phi_d = 0$) or presence ($\phi_d = 0.3$) of dislocations is distinguished by thin and thick lines, respectively, for each E_M value. Without dislocations, the result $\delta G \sim \cos(2\phi)$ is robust to interferometer parameter changes. The presence of dislocations affects *only* the cases of coupled MBSs, $E_M \neq 0$, by suppressing the $\phi_0/2$ harmonic in $G(\phi)$ in favor of the ϕ_0, which is always *odd*, that is, $\sin(\phi)$.

clearly that the asymmetry of $G(E)$ is controlled by the dislocations. The effect persists in the limit where the central ring is decoupled from the leads ($a = 0$): The spectrum of the ring is given by the solutions of $\cos(2E) = \cos(\pi\phi_d)$ and shows the symmetries $\{E_n(\phi_d)\} \neq -\{E_n(\phi_d)\}$ and $\{E_n(\phi_d)\} = -\{E_n(-\phi_d)\}$.

The general asymmetry features in $G(E)$ due to dislocations persist when MBSs are added, and new signature effects appear in the magnetoconductance as dislocations are manipulated. The $G(E)$ shows oscillatory behavior, with resonances at $\pm E_M$, shown in Fig. 2(a). In Fig. 2(b), we provide a summary of the dislocation effect on the behavior of $G(E)$. Introduction of nonzero dislocation phase causes a large asymmetry that persists for all values of E_M. If the flux ϕ is present, $G(E)$ becomes asymmetric at any value of ϕ_d, and more strongly as E_M increases (note that when MBSs are absent, there is no dependence on ϕ). The last observation was made also for a more complicated hypothetical interferometer.[11]

Figure 3 presents the characteristic influence of dislocations and Majorana states on the magnetoconductance at zero energy (i.e., zero voltage at low temperatures). As announced, even though TRS is broken by the MBS scattering, a resulting noneven $G(\phi)$ is observed only in the presence of dislocations. Namely, $\delta G(\phi)$ has two prominent Fourier components, and both have *definite parity*: The UCF in the form of $\sin(\phi)$ and the harmonic $\cos(2\phi)$. When $E_M = 0$ (MBS decoupled from each other), the UCF vanish. However, when $E_M \neq 0$, dislocations show a clear signature: In their presence, as E_M/Γ increases, the harmonic is suppressed in favor of the UCF, and therefore simultaneously the transformation from even to odd $G(\phi)$ is observed. If $E_M > \Gamma$, a small value of ϕ_d (e.g., 0.05) already causes a linear $G(\phi)$ up to $|\phi| \lesssim 1/4$ (cf. Fig. 3).

In conclusion, we demonstrated the usefulness of shear stress manipulated dislocations in observing neutral Majorana fermions in TIs. We found clear signatures of dislocation-MBS interplay in magnetoconductance oscillations at zero energy and showed the enhanced conductance symmetry of Eq. (1), a direct consequence of the symmetry of the TI and the presence of dislocations.

We thank A. Vishwanath, J. Bardarson, A. Akhmerov, and V. Juričić for useful discussions. A.M. is grateful for hospitality of E.-A. Kim. A.M. acknowledges financial support by the Nederlandse Organisatie voor Wetenschappelijk Onderzoek (NWO) and S.P. support by the DOE-BES through Grant No. DE-FG02-07ER46393.

[1] G. Moore and N. Read, Nucl. Phys. B **360**, 362 (1991).
[2] A. Kitaev, Ann. Phys. (NY) **303**, 2 (2003).
[3] N. Read and D. Green, Phys. Rev. B **61**, 10267 (2000).
[4] S. DasSarma, C. Nayak, and S. Tewari, Phys. Rev. B **73**, 220502(R) (2006).
[5] L. Fu and C. L. Kane, Phys. Rev. Lett. **100**, 096407 (2008); Phys. Rev. B **79**, 161408(R) (2009).
[6] J. Nilsson, A. R. Akhmerov, and C. W. J. Beenakker, Phys. Rev. Lett. **101**, 120403 (2008).
[7] A. Bernevig, T. Hughes, and S. C. Zhang, Science **314**, 1757 (2006); S. Murakami, Phys. Rev. Lett. **97**, 236805 (2006); L. Fu, C. L. Kane, and E. J. Mele, *ibid.* **98**, 106803 (2007); X.-L. Qi, T. L. Hughes, and S. C. Zhang, Phys. Rev. B **78**, 195424 (2008).
[8] L. Fu and C. L. Kane, Phys. Rev. B **76**, 045302 (2007).
[9] C. J. Bolech and E. Demler, Phys. Rev. Lett. **98**, 237002 (2007); G. W. Semenoff and P. Sodano, J. Phys. B **40**, 1479 (2007); S. Tewari, C. Zhang, S. DasSarma, C. Nayak, and D. H. Lee, Phys. Rev. Lett. **100**, 027001 (2008).
[10] L. Fu and C. L. Kane, Phys. Rev. Lett. **102**, 216403 (2009).
[11] C. Benjamin and J. K. Pachos, Phys. Rev. B **81**, 85101 (2010).
[12] R. M. Lutchyn, J. D. Sau, and S. Das Sarma, Phys. Rev. Lett. **105**, 077001 (2010).
[13] A. Mesaros, D. Sadri, and J. Zaanen, Phys. Rev. B **79**, 155111 (2009).
[14] Y. Ran, Y. Zhang, and A. Vishwanath, Nat. Phys. **5**, 298 (2009).
[15] M. Konig *et al.*, Science **318**, 766 (2007).
[16] S. Cole, A. F. Willoughby, and M. Brown, J. Mater. Sci. **20**, 274 (1985).
[17] A. Roth, C. Brüne, H. Buhmann, L. W. Molenkamp, J. Maciejko, X.-L. Qi, and S.-C. Zhang, Science **325**, 294 (2009).
[18] H. Kleinert, *Gauge Fields in Condensed Matter*, Vol. 2. (World Scientific, Singapore, 1989)
[19] X. Dai, T. L. Hughes, X.-L. Qi, Z. Fang, and S.-C. Zhang, Phys. Rev. B **77**, 125319 (2008).
[20] S. Chadov, X.-L. Qi, J. Kübler, G. H. Fecher, C. Felser, and S.-C. Zhang, Nature Materials **9**, 541 (2010).
[21] Y. Xia, D. Qian, D. Hsieh, L. Wray, A. Pal, H. Lin, A. Bansil, D. Grauer, Y. S. Hor, R. J. Cava, and M. Z. Hasan, Nat. Phys. **5**, 398 (2009).
[22] C. Xu and J. E. Moore, Phys. Rev. B **73**, 45322 (2006).
[23] C.-Y. Hou, E.-A. Kim, and C. Chamon, Phys. Rev. Lett. **102**, 76602 (2009); J. C. Y. Teo and C. L. Kane, Phys. Rev. B **79**, 235321 (2009).